Canonical molecular dynamics simulations for crystallization of metallic nanodroplets on MgO(100)

A. Jelea* and C. Mottet
CINaM, CNRS, Campus de Luminy, Case 913, 13288 Marseille Cedex 9, France

J. Goniakowski
INSP, CNRS-Université Paris 6, Campus de Boucicaut, 140 rue de Lourmel, 75015 Paris, France

G. Rossi and R. Ferrando
Dipartimento di Fisica dell'Università di Genova and CNISM, via Dodecaneso 33, 16146 Genova, Italy
(Received 27 November 2008; revised manuscript received 28 January 2009; published 28 April 2009)

The crystallization of Pd, Pt, and Ag nanodroplets in the range of 100–800 atoms (1.5–3 nm diameter) supported on the MgO(100) surface is simulated by canonical molecular dynamics (MD) using tight-binding many-body potentials for the metallic interactions and a potential-energy surface approach fitted to *ab initio* calculations for the metal-oxide support interaction. The simulations enable to determine the equilibrium supported shapes at finite temperature. These can be compared to the quenched MD simulations or global optimization searches for equilibrium shapes at 0 K. MD simulations at finite temperature after solidification do not display any evidence of a solid-solid transition. The structure is faced-centered cubic with atomic distortions and possible stacking faults. The morphology and epitaxial relation of nanoclusters with their support depend on the size and the nature of the metal: at small sizes (less than 200 atoms), all the metals adopt the (100) epitaxy and Ag clusters keep this epitaxy all over the size range. At 201 atoms (2 nm), Pd clusters are half (111)/half (100) whereas a majority of Pt clusters keeps the (100) epitaxy. At 405 atoms (2.5–3 nm) almost all the Pd clusters change to the (111) epitaxy whereas Pt clusters are half (111)/half (100). The size at which the transition from the (100) to the (111) epitaxy occurs is correlated with the lattice parameter misfit and to the difference in adhesion energy between the two epitaxies.

DOI: 10.1103/PhysRevB.79.165438 PACS number(s): 68.47.Jn, 61.46.Df, 68.35.−p

I. INTRODUCTION

Oxide-supported metal nanoparticles have given rise to a large amount of studies these last 20 years[1] notably because of their promising applications in heterogeneous catalysis.[2] We can notice important developments in the experimental control of their elaboration and characterization modes, from the observation of a single particle as performed by high-resolution transmission electron microscopy (HRTEM) (Refs. 3–5) or near-field microscopy (scanning tunneling[6–8] and atomic force microscopes[9,10]) to the *in situ* observation of a collection of nanoparticles with a sharp size distribution by grazing-incidence small-angle x-ray scattering (GISAXS).[11] For example, Pd nanoparticles supported on the MgO(100) surface have been both characterized by *ex situ* HRTEM (Ref. 12) and *in situ* GISAXS (Refs. 13 and 14) giving rise to comparative results between the two different techniques.[15,16] Notably, the experimental determination of the adhesion energy has been deduced from the measurement of the aspect ratio which is connected to energetic quantities of the system by the Wulff-Kaishew (WK) theorem.[17] The adhesion energy has been estimated to 1.12 J/m^2 by GISAXS and 0.91 J/m^2 by HRTEM, which can be compared to the direct theoretical estimation[18] of 0.90 J/m^2 in an atomistic approach, which couples *ab initio* calculations and statistic estimate of the equilibrium morphology of the nanoparticles using semiempirical potentials. The difference between experimental and theoretical results may be explained in terms of the lack of validity of the macroscopic Wulff-Kaishew theorem for small systems, as discussed in Ref. 18. Because of epitaxial strains (due to the misfit between the metal and the oxide), the adhesion energy evolves as a function of cluster size from 1 to 6 nm between 1 and 0.87 J/m^2 before converging to the value of 0.90 J/m^2 for which the Wulff-Kaishew theorem can reasonably be applied. There are also many experimental studies on Ag (Refs. 19 and 20) and Pt (Refs. 21 and 22) nanoclusters grown on MgO(100) substrates. All these studies confirm that the metal atom epitaxial site is located above the oxygen ions on the MgO(100) and the epitaxial orientation is (100) for Pd and Ag, whereas it changes from (100) to (111) as a function of temperature and growth conditions for Pt.[22]

All these experimental improvements helped the characterization of atomic structure, morphology, and epitaxy adopted by metallic nanoparticles grown on oxide surfaces. However, one of the important points which deserves further study is the nanoparticle formation process which can lead to nonequilibrium shapes due to the growth kinetics. In fact, such nanoclusters need a quite narrow range of thermal treatment to prevent Ostwald ripening, which would lead to the disappearance of smaller particles to the benefit of larger ones. An experimental solution to avoid this problem is to use nanostructured substrates where the clusters are trapped on ordered defects. This allows us to control their size dispersion.[23]

Realistic atomistic simulations are more and more useful in the study of these systems. Most of them are aimed at finding the most stable structures in the limit of $T=0$ K, so

that a direct comparison with experiments implies the assumption that there are no temperature effects on their structures. There is only a few papers on the effect of the temperature on the structure of supported nanoclusters. Oviedo *et al.*[24] employed pair potentials fitted on *ab initio* calculations to simulate relatively small Pd clusters (27, 45, and 64 atoms) supported on the MgO(100) surface at 300 and 1000 K and obtained clusters of a (partially disordered) truncated octahedral shape, characterized by (111)-oriented metal layers at the interface with the oxide substrate and an almost (001)-oriented topmost facet. Hernandez and Sanz,[25] with the same kind of potentials, described the deposition of Pd on α-Al_2O_3(0001) by classical molecular dynamics (MD) simulations. Finally San-Miguel *et al.*[26] demonstrated the influence of the temperature on the interaction between Pd clusters and the TiO_2 surface by first-principles MD simulations. We propose here to go beyond 0 K calculations, performing a characterization of the structure, morphology, and type of epitaxy of single Pd, Pt, and Ag nanoclusters at finite temperature. We use canonical MD simulations with tight-binding potentials for the metal-metal interactions and a potential-energy surface (PES) approach fitted to *ab initio* calculations for the metal-support interactions. To prevent possible kinetic trapping effects,[27] we start from high temperature, i.e., in the liquid state, and cool down the system with an extremely slow cooling rate, in order to approach equilibrium states.

The aim of this study is twofold: on one hand to demonstrate that canonical MD simulations of the recrystallization from a liquid nanodroplet can succeed to obtain equilibrium structures and notably those determined at 0 K (Refs. 28 and 29); on the other hand to compare directly finite-temperature simulated nanoclusters with experimental results, which are often obtained at relatively high temperature. In particular we concentrate on determining the nanoparticle structure (fcc or possible fivefold symmetry), its epitaxy on the MgO(100) support, and its aspect ratio as a function of clusters size.

The paper is composed of five sections. In Sec. II we describe the energetic model together with the canonical molecular dynamics simulations of the recrystallization of the metallic nanodroplets. In Sec. III, we show the results of these recrystallizations in terms of energy, atomic structure, epitaxy, and morphology for Ag, Pd, and Pt on MgO(100). In Sec. IV, we compare results with optimized structures at 0 K. In Sec. V, the results are discussed and some conclusions are given.

II. MODEL AND METHOD

The idea is to simulate the recrystallization of the metal nanodroplets supported on the MgO(100) surface through canonical MD with a temperature ramp starting from high temperature (liquid state) and cooling slowly the system. The simulation time at each temperature (a few 10^6 steps of calculation) must be sufficiently high to satisfy the ergodicity hypothesis in order to characterize equilibrium structures. As a consequence we use a quite simple semiempirical energetic model based on the second moment approximation (SMA) in the tight-binding (TB) scheme for the metal-metal interaction complemented by a many-body PES fitted to *ab initio* calculations of model metallic deposits on the perfect MgO(100) surface for the metal-oxide support interactions. While the many-body character of our potentials is a significant improvement with respect to earlier calculations based on pair potentials, the present energetic model implies several approximations in order to get an analytical formula allowing us to perform high-statistics calculations and notably to reach the equilibrium configurations for small clusters of a few nanometers. Among these approximations, one concerns the metallic interaction which is based on a many-body potential fitted to bulk properties that can become irrelevant for very low coordinated systems. We start here with systems of a hundred of atoms or more. The other drastic approximation concerns the oxide support that we consider as frozen. This approximation will be discussed in the following. Given these approximations, this study enables the thermodynamic treatment of the system where the statistical exploration of the phase space in time allows us to reasonably respect the ergodicity hypothesis.

A. Energetic model

The metal-metal interaction is modeled by a tight-binding semiempirical potential within the second moment approximation (TB-SMA) as formulated by Rosato *et al.*[30] The attractive part of the potential is derived analytically from the band energy in the framework of the tight-binding model, assuming a rectangular density of states fitted to the second moment of the actual density of states. Such model is particularly well suited to model transition and noble metals where the cohesion is governed by the *d*-electron band.[31] The attractive many-body term coming from the band energy for an atom at site n is given by

$$E_n^b = -\left\{ \sum_{m, r_{nm} < r_c} \xi^2 \exp\left[-2q\left(\frac{r_{nm}}{r_0} - 1 \right) \right] \right\}^{1/2}. \quad (1)$$

The stability of the system is ensured by adding a phenomenological core-repulsion term of the Born-Mayer type,

$$E_n^r = \sum_{m, r_{nm} < r_c} A \exp\left[-p\left(\frac{r_{nm}}{r_0} - 1 \right) \right]. \quad (2)$$

The total potential energy on site n is the sum of the band attractive term and the repulsive term,

$$E_n^{\mathrm{met}} = E_n^b + E_n^r. \quad (3)$$

In these expressions, r_{nm} is the distance between atoms at sites n and m, r_c is the cutoff radius of the interactions, and r_0 is the first-neighbor distance. The parameters ξ, q, A, p are fitted on bulk cohesive energy,[32] lattice parameter, and elastic constants.[33] They are given in Table I for a cutoff radius fixed to the third-neighbor distance: the above form of the potential is used up to the second neighbors, then the potential is smoothly linked to zero using a fifth-order polynomial between the second- and third-neighbor distances.

A few remarks on the potential used in this study are necessary. This is the most common version of the TB-SMA potential that can be compared to usual embedded atom

TABLE I. Parameters of the metallic potential. Pd* corresponds to the parametrization with the form of the potential extended to the third-neighbor distance and cutoff at the fourth.

Metal	ξ (eV)	A (eV)	q	p
Ag	1.19402	0.10433	3.190	10.790
Pt	2.50601	0.24241	3.680	11.140
Pd	1.70187	0.17149	3.794	11.000
Pd*	1.19237	0.05008	2.09	17.0

method[34] or effective-medium theory[35] potentials and allows us to reproduce qualitatively the main characteristics of the structure and morphology of the systems we consider, as will be shown in the following. However, one particularity of this kind of potential, when limited to the second neighbors, is to neglect the stacking fault energy or even stabilize this fault but with a very low energy ($1/10$ mJ m^{-2}, as shown in Table II). As this can have some consequences on the fine structure of the recrystallized clusters, we would like to check, by refitting the potential in order to increase this stacking fault energy, that the recrystallization procedure is not responsible of the possible stacking faults in the clusters. The new potential (TB-SMA^{3rd}) is extended up to the third neighbors (with cutoff at the fourth) in order to better reproduce the hexagonal compact (hcp) energy. It has been recently developed in the study of Ni/MgO(100) systems[38] and here it is applied to Pd. Such potential, nevertheless, underestimates the stacking fault energy as shown in Table II. The results obtained by density-functional theory (DFT) calculations, using plane-wave basis, ultrasoft Vanderbilt pseudopotentials, and the Perdew-Wang 91 exchange and correlation functional[36] as implemented in the Vienna *ab-initio* simulation package (VASP),[39] are given for comparison. As a conclusion, we show that we can improve and sophisticate the metal-metal potential in order to refine the results. However we would like to show that even the most simple version of the TB-SMA potential is able to catch the most important structural and morphological features of the systems under consideration.

For the metal-oxide part, there is no simple and reliable semiempirical potential as the one described above for the metal because of the different nature of the interactions in the two materials and of their interface.[40–42] DFT calculations have been used in order to better characterize the electronic structure and the energetics of the metal/MgO(100) interface.[43–49] In light of these studies, we know that the interaction is rather weak (physisorption type, decreasing from the middle to the end of the transition metal series), with a weak charge transfer and with a preferential adsorption on top of oxygen atoms.

TABLE II. Stacking fault energies in mJ/m^2 calculated using different methods: TB-SMA with a cutoff after the second neighbors (TB-SMA^{2nd}), with a cutoff after the third neighbors (TB-SMA^{3rd}), DFT with the Perdew-Wang 91 functional (Ref. 36) and experimental values from Ref. 37.

Metal	TB-SMA^{2nd}	TB-SMA^{3rd}	DFT	Expt.
Ag	−0.55		18	16
Pt	−0.23		263	
Pd	−0.27	49	110	180

However, even within the so-called *ab initio* approaches, the quantitative values do not always converge between the different methods [Hartree-Fock approach,[44] local-density approximation (LDA),[43,45] and generalized gradient approximation (GGA) (Ref. 45)]. Here, we perform systematic DFT calculations using ultrasoft Vanderbilt pseudopotentials in a plane-wave basis and with the GGA treatment which is better suited to describe the separated materials. We used in general the VASP code developed by the Vienna group.[39] Some of the calculations, performed by Barcaro and Fortunelli[50] on pentamer structure, used the plane-wave self-consistent field (PWSCF) code developed by the Trieste group.[51] We calculated by these first-principles methods a series of model pseudomorphic structures corresponding to one atom, one monolayer, and a thin film of five monolayers, varying the adsorption site (on top of oxygen atom, on top of magnesium atom, or in the hollow sites) as a function of the separation distance between the metal and MgO surfaces. The atomic structure has been relaxed in all these calculations, taking into account effectively the substrate relaxations. These model calculations are used to fit an analytical potential on the scheme of a PES.

At variance with the cases of Pd/MgO(100) (Ref. 52) and Pt/MgO(100),[22] the Ag/MgO(100) interface energy presents the particularity to evolve nonmonotonically as a function of silver coordination. This is correlated with the "metal-on-top" effect[53] for coinage metals, which additionally destabilizes the one-monolayer deposit as compared to the two-monolayer or pyramidlike pentamer cluster deposit. This justifies the choice of a pentamer in the fitting procedure of Ag/MgO(100).

Assuming a rigid PES approach,[52] the interaction energy between the metal deposit and the MgO(100) surface is a sum of the effective interactions of each metal atom at site n depending on the coordinates (x,y,z) and the number of first metal neighbors Z. The potential has a Morse-type dependence in z coordinate (the distance to the surface),

$$E_n^{\text{met-MgO}}(x,y,z,Z) = a_1(x,y,Z)\{e^{-2a_2(x,y,Z)[z-a_3(x,y,Z)]} - 2e^{-a_2(x,y,Z)[z-a_3(x,y,Z)]}\}$$

with an exponential dependence on the number of metallic neighbors (Z)

$$a_i(x,y,Z) = b_{i1}(x,y) + b_{i2}(x,y)e^{-Z/b_{i3}(x,y)}$$

and a periodic cosine function for the dependence in x and y coordinates parallel to the MgO(100) surface, with essentially three singular positions characteristic of the symmetry of this surface: above an oxygen atom, a magnesium atom, or an hollow site,

$$b_{ij}(x,y) = c_{ij1} + c_{ij2}\left\{\cos\left(\frac{2\pi}{a}x\right) + \cos\left(\frac{2\pi}{a}y\right)\right\} + c_{ij3}\left\{\cos\left(\frac{2\pi}{a}(x+y)\right) + \cos\left(\frac{2\pi}{a}(x-y)\right)\right\}$$

with $a = a_{\mathrm{MgO}}/\sqrt{2}$. This PES potential counts 27 different parameters c_{ijk} as given on the website.[54] The interaction of the metal with the MgO support is limited to the nearest layers of metal in contact with the oxide with a cutoff distance of $2a_{\mathrm{met}}$, where a_{met} is the lattice parameter of the metal. This allows us to link this potential to zero without a large discontinuity as we could have if we took only the first metal layer. Knowing that DFT calculations integrate the full adsorption energy without cutoff, this cutting distance can lead to some possible overestimates of the interaction. Nevertheless, as the interaction is rapidly damped with the distance to the support, it does not lead to significant overestimate.

Finally, the total energy of the supported cluster of N metal atoms is a sum of the contributions of the metal-metal and metal-oxide interactions,

$$E_{\mathrm{tot}} = \sum_{n=1}^{N} E_n^{\mathrm{met}} + E_{n,}^{\mathrm{met\text{-}MgO}}. \quad (4)$$

Even if the two energetic terms are added in a pairwise way, the many-body character of the metallic bonding and its effect on the adsorption energetics on the oxide support are taken into account effectively in the fitting procedure of the PES approach.

The approximation of a rigid oxide surface (no atomic relaxation in the substrate) has been justified by quantitative calculations of the energetic cost of the tetragonal deformation of either the Pd or MgO lattice.[55] It comes out that it costs clearly less energy to strain the metal than the oxide. This justifies neglecting in a first approximation the substrate deformation. In the following, we discuss the frozen aspect of the substrate in the molecular dynamics simulations.

B. Simulation method

The phase transition from solid to liquid or liquid to solid by slow heating or cooling of metallic clusters on MgO(100) is studied by canonical molecular dynamics simulations. These simulations allow us to calculate the average total energy over a large quantity of configurations. The temperature is maintained constant by an Andersen thermostat,[56] which couples the cluster to a heat bath (here the MgO substrate). The bath causes stochastic collisions generating a Maxwell-Boltzmann distribution of the velocities. Between two stochastic collisions, the system evolves according to the classical Newton's equations, which are numerically solved by the velocity Verlet algorithm.[57] The instantaneous temperature fluctuates as shown in Fig. 1 but the average temperature is well converging, in an interval of tens of ns. The temperature is increased (decreased) according to a heating (cooling) rate typically equal to (−)0.5 K/ns or less, equivalent to a few 10^6 steps of molecular dynamics each 10 or 20 K. In our energetic model, the MgO(100) substrate is rigid and the atomic vibrations are transmitted to the cluster via its interfacial plane where are locally applied the stochastic collisions of the Andersen thermostat. We checked that this method is almost equivalent to the surface oscillator model used in molecule-surface phonon coupling.[58] In this model, the motion of surface atoms is described through three-dimensional harmonic oscillators with amplitude and frequency fitted to *ab initio* calculations.

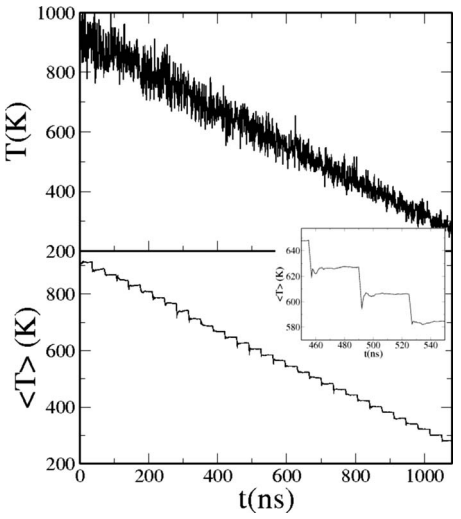

FIG. 1. Instantaneous temperature (top graph) and average temperature (bottom graph) as functions of the simulation time (the time step in the simulations is 7 ps) following the ramp in temperature for the successive canonical molecular dynamics simulations. The inset zooms on a part of the average temperature curve.

The melting and recrystallization curves are displayed in Fig. 2 where we started from a free isotropic truncated octahedron put on the MgO(100) substrate at room temperature. Then, by slowly increasing the temperature, the surface diffusion makes the cluster morphology change from the free shape to the supported shape.[59] This is a solid-solid transition. Then the second transition consists in the global melting

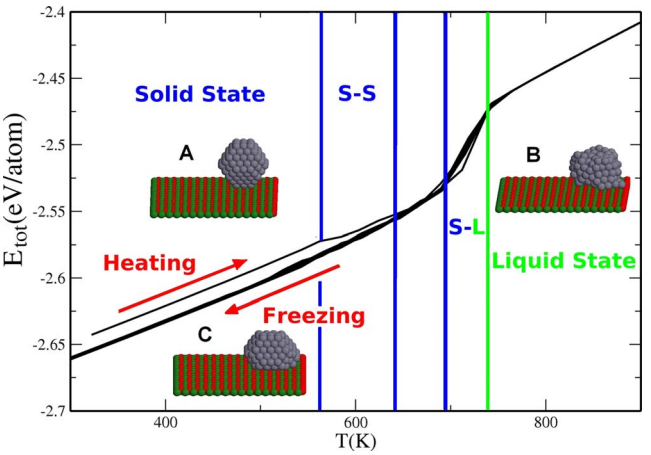

FIG. 2. (Color online) Typical caloric curves of the heating of the metal nanocluster with its free isotropic shape (a) as deposited on the MgO(100) substrate, then solid-solid transformation toward its supported equilibrium shape, (b) then solid-liquid transition to the nanodroplet, then cooling, recovering of the supported shape (c) after recrystallization.

of the cluster. By slowly cooling the system, it recrystallizes in its supported shape which is comparable, as we will see later, to its equilibrium morphology as predicted by the global optimization method. We notice that there is no hysteresis in the recrystallization process, contrary to what can be seen for larger-size systems.[60] The total energy reported on these curves is the averaged energy over a large number of time steps (a few 10^6) after the equilibration of the temperature, as shown in Fig. 1.

In order to compare our simulated clusters to the optimized ones (either by global or local optimization at 0 K), we have quenched the final structures obtained at finite temperature to 0 K using quenched molecular dynamics in microcanonical ensemble. This procedure allows us to relax the atomic positions to get the nearest local minimum structure.

C. Order parameters

We define here all the different structural order parameters which are averaged at each temperature in our simulations. One parameter concerns the epitaxial orientation which can be characterized by the coordination number of the atoms located at the interface,

$$Z_{\text{int}} = \frac{1}{\tau}\sum_{t=t_0}^{t_0+\tau}\frac{1}{N_{\text{int}}}\sum_{i=1}^{N_{\text{int}}} Z_i(t), \tag{5}$$

where τ is the number of time steps at each temperature (typically 5×10^6 steps equivalent to 35 ns in time, with t_0 being the time after which the temperature is equilibrated by the thermostat) and N_{int} is the number of atoms of the cluster at the interface with the MgO(100) substrate.

The other local order parameters are derived from the common neighbor analysis (CNA) proposed by Honeycutt and Andersen[61] and further developed by Faken and Jonsson.[62] It consists in a decomposition of the radial distribution function according to the environment of the pairs of atoms sharing common neighbors. Basically, the CNA signature defined for each pair of nearest neighbors is composed of three integer number (nbp) representing the number of common neighbors (n), the number of bonds between shared neighbors (b), and the number of bonds in the longest bond-path formed among the shared neighbors (p). Within this classification we can distinguish without any ambiguity the fcc, hcp, or fivefold symmetry [icosahedral (Ih) or decahedral (Dh)] with the (421), (422), or (555) signature. This applies to bulklike atom pairs, as those which are inside the cluster. On the other hand, surface atoms present broken bonds, so that other CNA signatures come into play, such as the (311) signature on (111) facets and the (211) signature on (100) facets. All these signatures are averaged in time and space inside the cluster in order to give a reliable quantity characteristic of an equilibrium configuration, as described in Eq. (5).

Finally, the last parameter which typically characterizes the morphology of the clusters and which can be directly compared to experimental results[7,15,16,20] is the aspect ratio. It can be defined according to the WK geometrical construction[17] for the two different epitaxies:

(i) In the (100) epitaxy, $R_{(100)}=h/2h_A$, with h being the height of the cluster, perpendicularly to the substrate, and h_A being the distance between the center (as defined in the Wulff shape if the cluster was prolonged symmetrically inside the substrate) to the (100) top facet. From the WK theorem, at equilibrium, the width of the cluster at its base is equal to $2h_A$ (see Ref. 18), and we can link the geometrical aspect ratio to the energetic quantities as follows:

$$R_{(100)} = 1 - \frac{\beta_{(100)}}{2\gamma_{(100)}}, \tag{6}$$

where $\beta_{(100)}$ is the adhesion energy per unit area of the cluster on the surface and $\gamma_{(100)}$ is the (100) surface energy. This relation, essentially derived for a macroscopic crystal on a support in analogy to the Young-Dupre equation for a liquid supported droplet, can be extended to relatively small clusters[18] (6–8 nm).

(ii) In the (111) epitaxy, $R_{(111)}=h/w$, with w being the width of the top (111) facet. Following the WK theorem, we can link this geometrical parameter to the energetic quantities as detailed in Ref. 7,

$$R_{(111)} = \sqrt{\frac{2}{3}}\frac{2\gamma_{(111)} - \beta_{(111)}}{\gamma_{(100)}}. \tag{7}$$

III. RESULTS AND ANALYSIS OF THE RECRYSTALLIZATION

Pd, Pt, and Ag nanodroplets have been slowly cooled and recrystallized giving some ordered crystalline nanoclusters mostly with the fcc structure and different epitaxial orientations depending on the size and the type of metal. The two epitaxial orientations are the (100) [the same as the MgO(100) substrate] and the (111), as shown in the top left of Fig. 3. For each cluster, from 10 to 20 molecular dynamics simulations have been performed in each case in order to accumulate statistics. We found very few fivefold symmetry clusters (only two cases for small Pt clusters), even though most of the free clusters at small sizes (see Fig. 3) present fivefold symmetries.[27] By performing the recrystallization in the same conditions on a free (unsupported) Ag droplet of 201 atoms, we obtained 100% of fivefold symmetry structures: mainly Dh and a few Ih clusters. In any case we have encountered clusters in which orientation of atomic layers changes from (111) at the interface toward (100) at the topmost facet, as reported by Oviedo *et al.*[24] Our results confirm that the substrate imposes its symmetry to the supported clusters as we have already concluded in the case of Pd/MgO(100) nanoclusters.[59] In Secs. III A and III B we will detail the epitaxial orientation of the nanoclusters, their structure, and morphology.

A. Epitaxial orientations of the nanoclusters

The epitaxial orientations are illustrated in Table III, where the percentage of (100) epitaxy clusters is reported, with the other clusters being in (111) epitaxy. The Dh Pt clusters which have been obtained at 90 and 201 atoms adopt

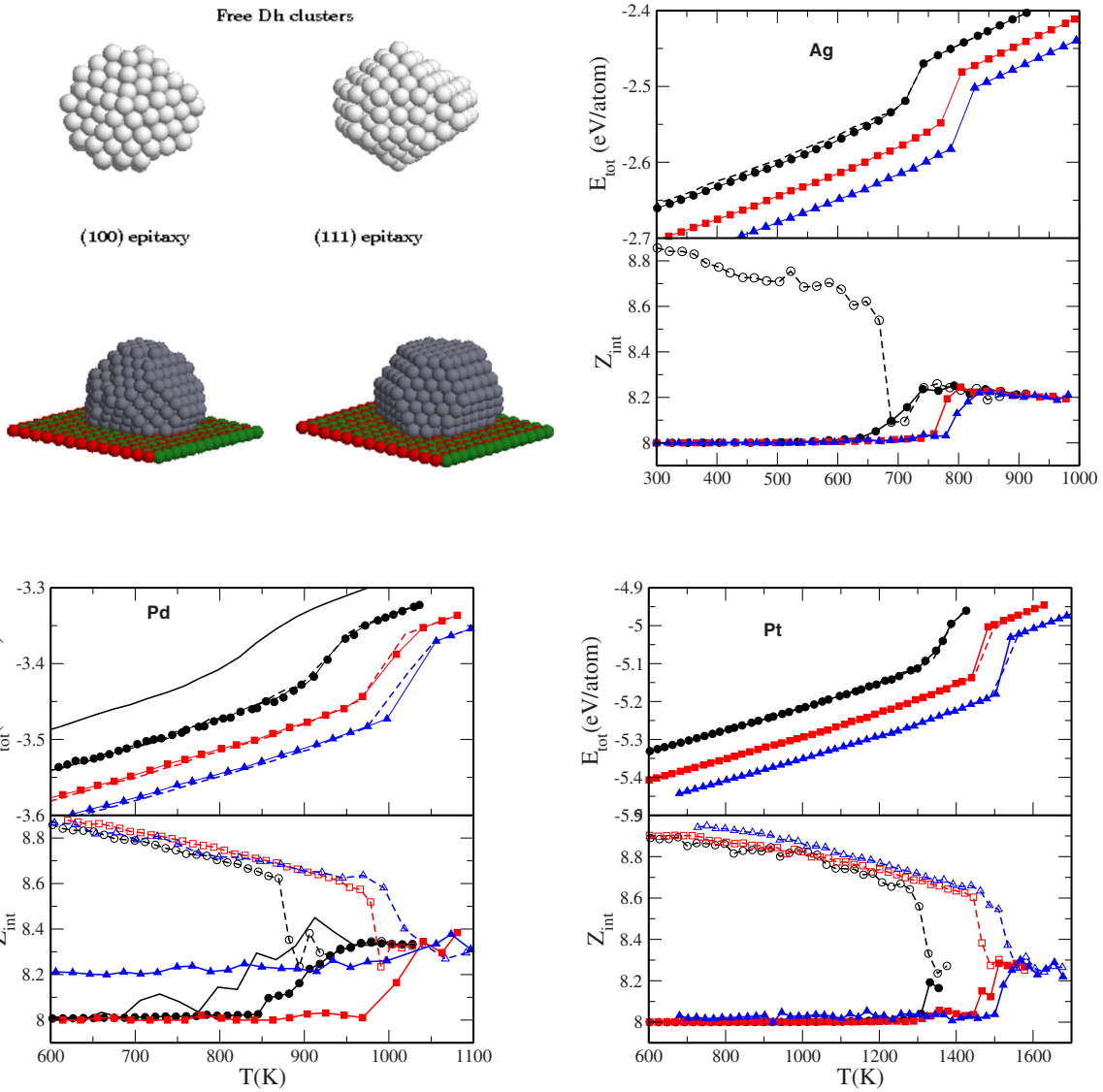

FIG. 3. (Color online) On the top left, unsupported clusters with the decahedral structure (two views) and the two kinds of epitaxial structures for supported clusters depicted with atomic representation are shown. All the graphs represent the caloric curves and their associated average Z_{int} for the recrystallization of Ag, Pd, and Pt clusters of 201 atoms (black circle), 405 atoms (green square), and 807 atoms (blue triangle). In the Pd case, the full line represents the 91-atom cluster. The dashed lines represent the (111) epitaxial structures and the full lines represent (100).

a pseudo-(100) epitaxy so they are counted in the (100) epitaxy. In the Ag case, almost all the runs lead to the (100) epitaxy for all sizes, with the single exception of a (111) epitaxy cluster of size 201. In the Pt and Pd cases, the percentages are much more equilibrated, and we observe a transition from the (100) epitaxy at small sizes to the (111) epitaxy at larger sizes, as follows from the results at 405 atoms for Pt and at 201 atoms for Pd. Such results are in very good

TABLE III. Percentages of the (100)-oriented epitaxial clusters for different cluster sizes: N is the number of atoms. In parentheses, we indicate the total number of runs. The last column indicates the critical size of the transition [N_c obtained by 0 K optimization methods (Refs. 28 and 29)].

Metal	N=91 at. (%)	N=201 at. (%)	N=405 at. (%)	N=807 at. (%)	N_c (0 K) (at.)
Ag	100 (10)	90 (10)	100 (10)	100 (7)	>3000
Pt	100 (10)	70 (20)	50 (20)	40 (7)	500–600
Pd	100 (10)	60 (20)	10 (10)	10 (7)	200

agreement with the direct optimization at 0 K performed by global optimization methods at small sizes ($N<500$) or by comparison of selected structural motifs for large sizes ($N<3000$).[28,29] The critical size for the transitions have been reported in Table III. The silver clusters at 0 K are essentially (100) along the whole range of size from 100 to 2800 atoms.[28] The Pt clusters are (100) at size lower than 400 atoms. At $N=400$, 403, 404, and 407, the global minima have the (111) fcc structure, whereas at $N=405$ and 406 the global minima are (100) fcc.[29] This is in very nice agreement with our statistic performed on 405 atoms Pt clusters over 20 runs finding exactly 50% (100) and 50% (111) epitaxies. At 807 atoms, the two structures are still competing, with a slight indication for the (111) to be favored. For Pd, the inversion between the majority of (100) epitaxies at small sizes ($N\leq 201$) and the majority of (111) epitaxies at large sizes takes place around 200 atoms which is in very nice agreement with the 0 K optimization results.

The caloric curves and the associated coordination number at the interface Z_{int} are illustrated in Fig. 3. The curves represent the average over the different simulations performed at each size. We notice that the liquid-solid transition is well connected to the change in the coordination number, which is eight for the (100) epitaxy or nine for the (111) epitaxy. There is no epitaxial change after the recrystallization since Z_{int} is relatively constant in the temperature range considered and there is no noticeable change in the slope of the caloric curves. This indicates that there are no solid-solid transitions. In the silver case, all clusters are in (100) epitaxy except one case where the cluster of 201 atoms adopts the (111) epitaxy. In the Pd case, we note that the Z_{int} curve for the size of 91 atoms is quite irregular even after averaging over ten simulations. In fact, as the size is very small, the liquid-solid transition is very smooth and the number of atoms at the interface itself can fluctuate, which makes the average coordination number at the interface not stable at least beyond a temperature of 700 K.

Another remark concerns the small oscillations of Z_{int} for the clusters of 201 and 405 atoms in the (111) epitaxy (dashed lines in the Pd Z_{int} curve of Fig. 3) at the beginning of recrystallization: some of these structures oscillate between the coordinations 8 and 9. A small majority (60%) chooses the (100) epitaxy for the 201 atoms size and a large majority (90%) chooses the (111) epitaxy for the 405 and 807 atoms sizes. Looking at the energy curves, we can check that when the percentages are quite similar, the energies are similar, whereas when the percentages are in favor of one epitaxy, as in the case of Ag_{201}, Pd_{405}, and Pd_{807}, this epitaxy corresponds to a clearly lower energy. For Pd_{807}, the (100) epitaxy is not stable (only one case over seven trials) and presents a coordination number at the interface higher than 8 because of the presence of stacking faults inside the cluster, leading to a (111) local environment at the interface. In our cooling simulations, we find the same dislocated cluster as the one obtained by geometrical optimization at 0 K by Vervisch *et al.*[52] There, only the (100) epitaxy was considered. We show here that with the same potential, the (111) epitaxy is favorable, avoiding the misfit dislocations appearing at size larger than 3 nm in the (100) epitaxy.[52] Finally in the Pt case, the two kinds of epitaxies are quite equilibrated with percentages near 50% for 405 and 807 atoms sizes (see Table III) and the caloric curves of Pt in Fig. 3 present quasi-degenerate energies for the two epitaxies.

We can conclude at this point that since we recover the same type of epitaxy as the one determined by 0 K optimizations (the full comparison of the structures is performed in Sec. IV), and as there is no evident solid-solid transition in the temperature range covered by our simulations, this recrystallization process seems efficient to characterize equilibrium structures at finite temperature. This is not a rigorous proof because we cannot exclude that there are no other lower-energy structures that the simulations did not explore. We will characterize in the following other structural and morphological parameters at finite temperature.

B. Structure and morphology during the recrystallization

We followed the internal structure and the morphology of the clusters all along their recrystallization process by calculating the mean values of the CNA local order parameters. (421) and (422) signatures are characteristic of the internal structure of the clusters whereas (311) and (211) signatures are characteristic of the surface sites giving some information on their morphology. The curves in Fig. 4 give these signatures for Ag and Pt clusters of 405 atoms as a function of the temperature. The liquid-solid transition is characterized by the strong variation of the CNA parameters, which is well correlated with the transition observed in the caloric curves. The (421) signature applies to all nearest-neighbor pairs in the fcc bulk crystal, so that it is majority in the perfectly recrystallized clusters. The discrepancy between the bulk (100%) and the cluster (70%) (421) percentages comes from the surface sites of the cluster and depends on the cluster size (i.e., the surface to core sites ratio). The (422) signature applies to 50% of the pairs in the hcp bulk, with the other 50% belonging to the (421) signature. The presence of the (422) signature means there are some hcp/fcc stacking faults in the cluster. We only see two cases of the (555) signature in supported clusters, both on small Pt clusters.

In the Ag case, only one (100) epitaxial cluster has a pure fcc structure: it does not display any (422) signature. All the other clusters display nonzero (422) percentages which are characteristic of some hcp/fcc stacking faults. Such defects are illustrated in Fig. 5. The higher the (422) percentage, the higher the number of atom pairs with a hcp environment. For example, the defective cluster whose curve is in the vicinity of the perfect one displays only one hcp stacking facet [a (111) facet in hcp position] whereas when the stacking fault lies inside the cluster, the (422) signature reaches at least 10% and (421) decreases to 60% or less.

If we consider the (421) and (422) signatures of Pd and Pt clusters, as compared to Ag, we notice that the (100) epitaxial clusters have similar signatures, i.e., localized around 60% for the (421) and 10% for the (422) signatures, which means that their structures presenting a single stacking fault are comparable. The stacking faults in the (111) epitaxial structures are not lateral as in the (100) epitaxy but parallel to the substrate. (111) epitaxial clusters have generally higher (422) and lower (421) signatures, which indicates a larger

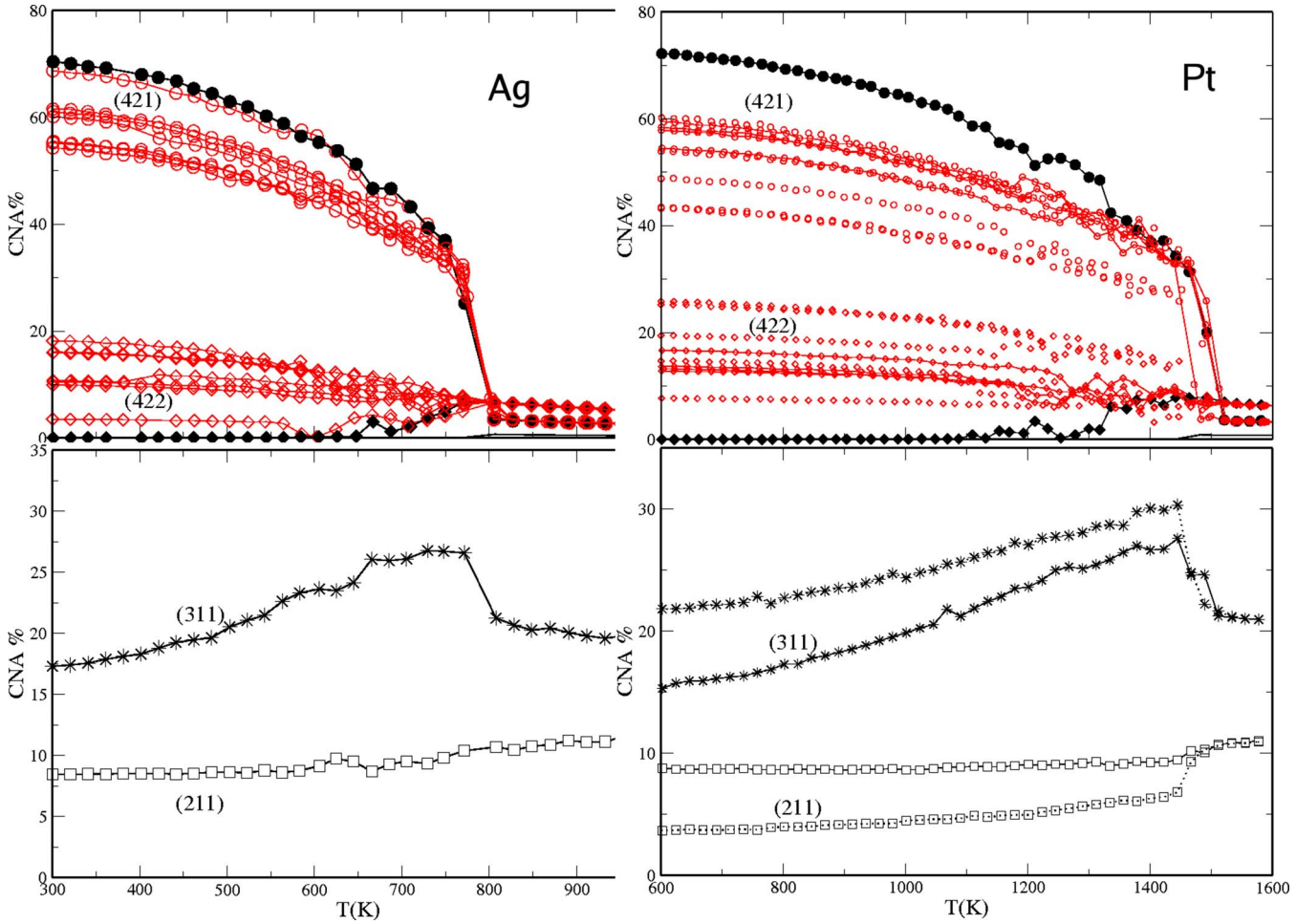

FIG. 4. (Color online) CNA signatures characteristic of the internal structure (top graphs) and morphology (bottom graphs) for Ag and Pt clusters of 405 atoms [(100) epitaxy with a continuous line and (111) epitaxy with dashed line]. The (421) and (422) signatures in the top graph represent, respectively, the fcc and hcp symmetries. Black circles correspond to the perfect fcc structure [i.e., maximum of the (421) signature and no (422) signature]. The others curves in red display stacking faults in various quantities. The (311) and (211) signatures in the bottom graphs represent, respectively, the (111) and (100) facets for the (100) epitaxy in the case of Ag and in both the (100) and the (111) (dashed line) in the case of Pt.

quantity of stacking faults in this orientation, especially in the case of Pt. We can also mention that in the Pt clusters of 201 atoms or in one trial of the Pd clusters of 807 atoms, we get a completely hcp ordered cluster with 30%-30% of each signature. However these clusters do not present a high stability as it was the case for the Ni/MgO(100) system described by Ferrando *et al.*[38] In the case of Pd, we obtained a single undefected cluster with (111) epitaxy. Using the potential extended to the third neighbors (as detailed in Sec. II) allows us to recover a large quantity of undefected clusters as illustrated in Fig. 6 for Pd, thus demonstrating the efficiency of the recrystallization procedure to get the minimum energy structures as a function of the potential used.

The morphology of the clusters is characterized by the (311) and (211) signatures displayed in the bottom graphs of Fig. 4. Ag(100) epitaxial clusters display a majority of (311) signatures which are characteristic of the (111) facet sites and less (211) signatures characteristic of the (100) facets. In Pt (and Pd) clusters, both (100) and (111) epitaxies lead to a majority of (311) signatures [i.e., a larger extension of the (111) facets compared to (100)] but we notice also that the (111) epitaxy presents even more (111) facets. Such epitaxy optimizes the surface energy of the clusters since the (111) facets have a lower surface energy than the (100) ones.

To completely characterize the clusters morphology, we finally calculate the aspect ratio as a function of the temperature to control its stability during the recrystallization process. We can see in Fig. 7 for Pd and Pt clusters of 201 atoms that it is relatively convergent. At high temperature, the values of $R_{(100)}$ and $R_{(111)}$ in the liquid phase are different be-

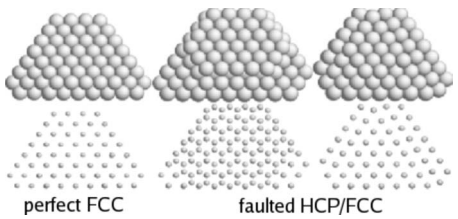

FIG. 5. Perfect fcc cluster and hcp/fcc faulted cluster with two views rotated from 90°.

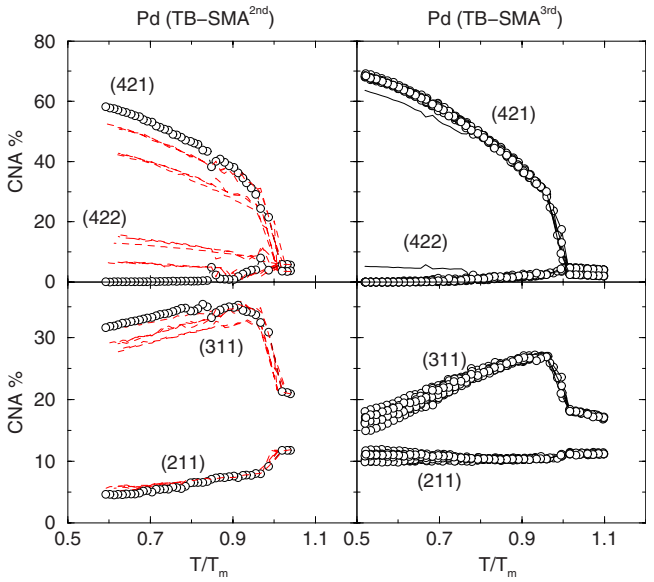

FIG. 6. (Color online) CNA signatures as in Fig. 4 for the 405-atom Pd clusters with the different parametrizations of the TB-SMA potentials.

cause of their definition from the solid state, whereas the nanodroplets are basically identical. At lower temperature, $R_{(100)}$ converges toward two possible values (both in Pd and in Pt), with the lower one being systematically in good agreement with the one determined at 0 K on optimized structures as given in Table IV. $R_{(111)}$ gives one convergent value for Pd. This value is larger as compared to the optimized morphology at 0 K (0.5 compared to 0.42). For Pt, two values are found with the lower one (0.7) equal to what is obtained at 0 K. We will compare in Sec. IV these values with the ones predicted by the WK construction.[17]

IV. COMPARISON WITH OPTIMIZED STRUCTURES

The structures obtained by recrystallization have been subsequently locally optimized using quenched molecular dynamics in order to compare their energy to the one obtained by global optimization methods at 0 K.[28,29] The specific surface energy of the supported cluster is described by the parameter $\Delta=(E_{\mathrm{tot}}-NE_{\mathrm{coh}})/N^{2/3}$ which is plotted in Fig. 8 together with its decomposition in the metal-metal contribution ($\Delta_{\mathrm{m\text{-}m}}$) and the metal-support adhesion energy ($E_{\mathrm{m\text{-}MgO}}$). The metal-metal contribution is well correlated with the number of dangling bonds i.e., the number of bonds to be cut in order to "extract" the cluster from the bulk. It is given by $Z_{\mathrm{cut}}=\Sigma_{i=1}^{12} n_i(12-i)$, where n_i is the number of atoms with the coordination number i. The higher the number of dangling bonds the higher the $\Delta_{\mathrm{m\text{-}m}}$ parameter and the lower the stability of the unsupported metal clusters. We have seen previously, thanks to the comparison of the (311) and (211) signatures, that the (111) epitaxial clusters have more (111) facets than the (100) epitaxial ones. The (100) facets atoms being coordinated by 8 and the (111) by 9, the (111) epitaxial clusters have globally less dangling bonds than the (100) ones. Thus they minimize the $\Delta_{\mathrm{m\text{-}m}}$ as can be seen in Fig. 8, middle row.

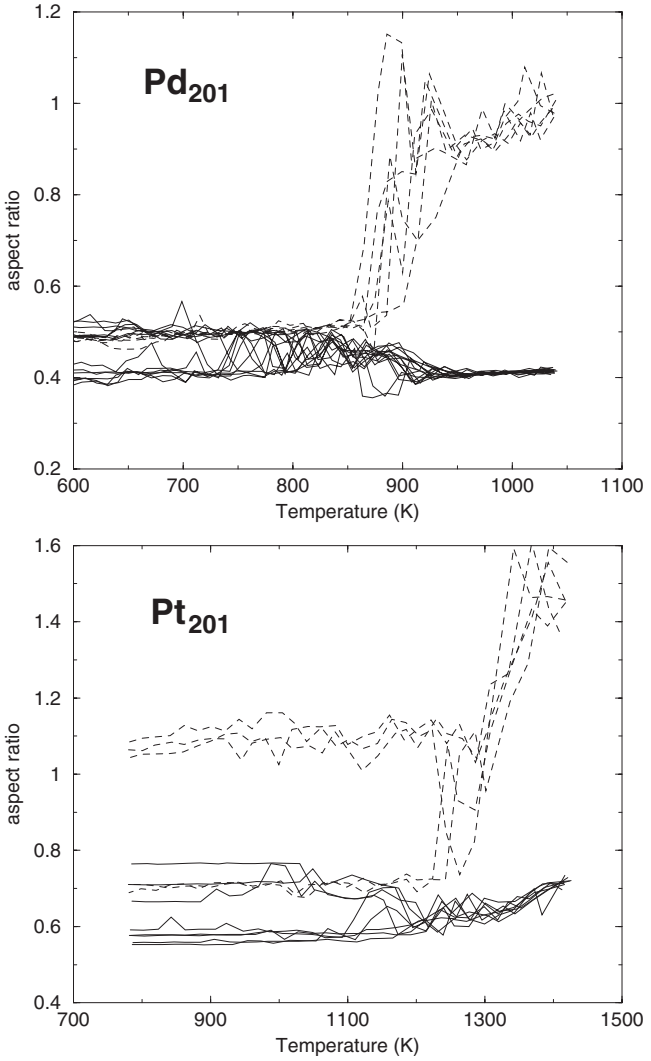

FIG. 7. $R_{(100)}$ and $R_{(111)}$ aspect ratios corresponding to the (100) and (111) epitaxial structures, respectively, with continuous line and dashed line.

The interaction with the support allows us to partially neutralize the dangling bonds. The strength of this interaction decreases with the coordination number of the metal atoms at the interface. Thus the less coordinated atoms from a (100) facet interact stronger with the MgO (100) support than the atoms in (111) facet. Moreover, the (100) epitaxy may produce a pseudomorphic relation with the MgO(100)

TABLE IV. Aspect ratio after recrystallization and their estimation by the WK construction using surface and interface energies given in Table V.

Metal	$N=201$	$N=405$	$N=807$	WK
Ag $R_{(100)}$	0.65	0.60	0.56	0.71
Pt $R_{(100)}$	0.57	0.70	0.55	0.70
Pt $R_{(111)}$	0.70	0.81	0.81	0.96
Pd $R_{(100)}$	0.38	0.46	0.40	0.44
Pd $R_{(111)}$	0.42	0.47	0.67	0.55

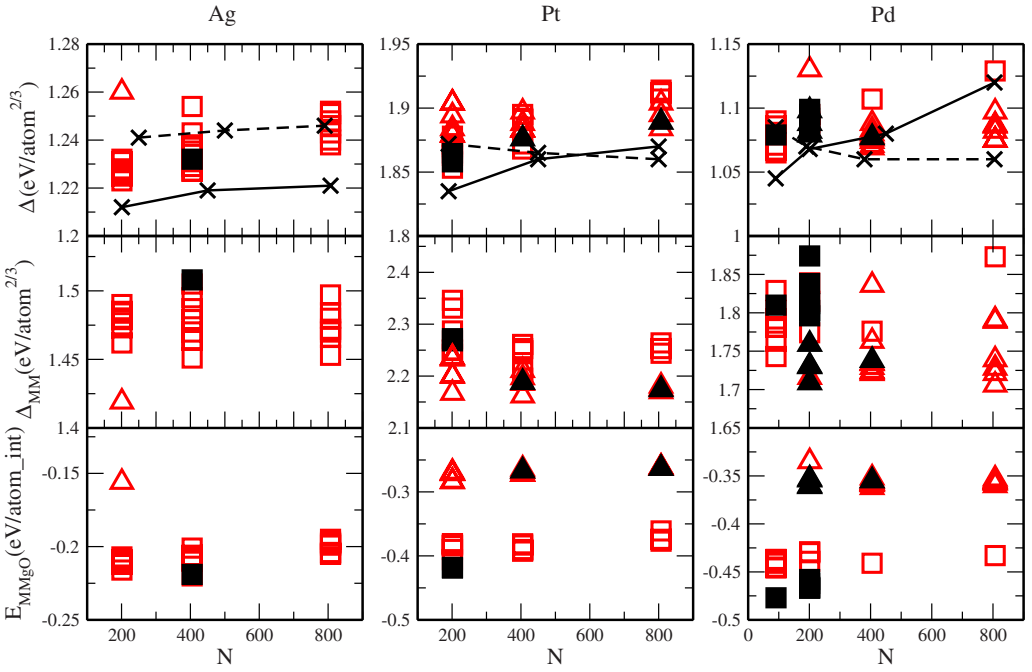

FIG. 8. (Color online) Specific surface energy Δ for the metal clusters: top row is the global quantity, middle row is the metallic interaction part, and bottom row is the adhesion to the support part. The squares represent the (100) epitaxy and the triangles represent (111). The structures with hcp/fcc stacking faults are in open red symbols whereas the perfect fcc structures are in black. The crosses represent the results obtained by global optimization (Refs. 28 and 29): continuous line for the (100) epitaxy and dashed line for the (111).

substrate, which of course improves its adhesion. All these factors favor the (100) epitaxy as compared to the (111) and it is clearly illustrated in Fig. 8, bottom row where $E_{\text{m-MgO}}$ of the (100) epitaxy is well below the one of the (111) epitaxy.

These two contributions are opposite, and the stability of one of the two epitaxies is ruled by a subtle balance between the two. This balance depends essentially on the cluster size and on the metal. Indeed, the anisotropy between (111) and (100) surface energies is metal dependent (lower for Ag and increasing from Pd to Pt) as well as the adhesion, which is weaker for noble metals and stronger for Pd and Pt. The other metal-dependent parameter is the lattice misfit with the MgO(100) substrate which induces a lattice deformation of the deposited metal in order to optimize the adhesion energy. Once again it is small for Ag (3%) and larger for Pt (7%) and Pd (near 8%).

Things are quite simple for Ag since the (100) epitaxy is the most stable within the whole size range from 200 to 800 atoms.[28] Both $\Delta_{\text{m-m}}$ and $E_{\text{m-MgO}}$ are weak but the (100) adhesion energy is the driving force. This is well reproduced by our recrystallizations results which gave only this epitaxy.

For Pt and Pd the situation is different: for small sizes, less than 400 atoms for Pt and 200 atoms for Pd, the (100) epitaxy is the most stable, as we found by recrystallization, then the (111) epitaxy becomes more stable. The two factors responsible of this epitaxy change are the lattice misfit and the variation of the adhesion energy as a function of size. For the (100) epitaxy, at small sizes, each metal atom is located above an oxygen atom (the most stable adsorption site for the metal atoms) which requires straining the metal cluster. The elastic energy to strain the cluster increases with cluster size. At a certain size, the cluster releases its strain, recovering its lattice parameter, which leads to the loss of the lattice coherence between the cluster and its substrate, and corresponds to the introduction of interfacial dislocations destabilizing the interface by a weakening of its adhesion energy.[52] But these dislocations take place for very precise sizes, given by the Vernier rule, i.e., around 3.5 nm for Pd and 4 nm for Pt, which are much larger than the transition observed here. Another way to reduce the strain at the interface is by changing the epitaxy: from (100) to (111). A small difference between the adhesion energies of the two epitaxies facilitates the (100)-(111) transition. Pd has a larger misfit and a smaller difference in adhesion energy. As a consequence, the (100)-(111) transition appears at a smaller size for Pd. Ag has a very small misfit and consequently does not change in epitaxy within the studied range.

The comparison of the aspect ratio calculated at 0 K as a function of cluster size with the predictions of the WK construction is given in Table IV (using the surface and interface energies given in Table V). These results show that the WK construction is not completely realistic for small sizes because of two reasons: first, as the clusters size decreases, the discretization of the length (h) as a function of the number of atomic planes becomes sensible,[59] modifying significantly the aspect ratio value at small sizes; second, the adhesion energy varies with cluster size because of epitaxial strain leading to a variation of the aspect ratio with cluster size.[18] As a consequence, we notice that the aspect ratio of our optimized Ag clusters is smaller (around 0.6) than the one predicted by the WK construction (0.7), within the energetic values of our model. However, it is in a quantitative agreement with experimental measurements performed on nanoparticles in a size range of 1–2 nm by GISAXS,[20] which

TABLE V. Energetic quantities in J/m^2 for extended (infinite) surfaces or interfaces.

Metal	$\gamma_{(100)}$	$\gamma_{(111)}$	$\beta_{(100)}$	$\beta_{(111)}$
Ag	0.658	0.584	0.38	0.29
Pt	1.146	0.985	0.68	0.63
Pd	0.818	0.706	0.91	0.86

found an aspect ratio comprised between 0.5 and 0.6. We would like to point out here the risk of using the WK construction in order to determine experimentally the adhesion energy, without taking into account a possible deviation coming from size effects. We cannot pretend to predict the right value of the aspect ratio because of the approximations we used, notably in what concerns the TB-SMA potential which underestimates the metal surface energy, whereas the adhesion energy coming from the *ab initio* calculations is more realistic. As a consequence, the aspect ratio, which depends on both quantities, is not quantitatively relevant in absolute value. But its variation as a function of clusters size as compared to the WK estimate within the same energetic model is significant.

As the surface energy is relatively constant as a function of clusters size, the adhesion energy is the main parameter susceptible to change as a function of clusters size. Such variations of the aspect ratio are also noticeable in the case of Pt and Pd giving in general smaller values for small clusters as compared to the WK estimation. This is coherent with a strengthening of the adhesion energy at small size leading to a flattening of the clusters. If the qualitative tendency of our model is right, the comparison with experimental values can be misleading. This is the case for Pd where the experimental result of 0.6 has been obtained in the same kind of experiment as in Ag case.[16] In such case, we know that the Pd surface energy of our model is underestimated, so that using the same adhesion energy ($0.9\ J/m^2$), we necessarily underestimate the aspect ratio, which is what we obtain (Table IV). Also we know that by improving the Pd surface energy, as it was the case in a precedent study[18] or by using the TB-SMA extended to the third neighbors, we increase the aspect ratio from around 0.55 to 0.7 in a very nice agreement with experimental results. In the case of silver, the good agreement between our model and the experiments could come from a double compensation: the weak (100) surface energy of the metal in the TB-SMA model ($0.66\ J/m^2$ instead of $1.24\ J/m^2$ experimentally or by DFT calculations) seems to be compensated by a weak adhesion energy as calculated by DFT calculations ($0.38\ J/m^2$ as compared to $0.83\ J/m^2$ obtained by Hartree-Fock calculations[63]). Knowing that the *ab initio* calculations give different results in that case, it is difficult to go further in the comparison, but we would like to emphasize that taking the experimental measurement of the aspect ratio of small clusters (1–2 nm) and applying the WK construction we can deduce a higher value than the infinite interfacial adhesion energy of the system because of size effects to be considered in small nanoclusters.

V. DISCUSSIONS AND CONCLUSIONS

The crystallization of Ag, Pt, and Pd nanoclusters supported on the MgO(100) surface has been simulated using canonical molecular dynamics within a semiempirical potential model. The statistics on the crystallized structures allows us to determine the stable structure depending on the cluster size and on the metal. In particular, the type of epitaxy between (100) and (111) and the morphology of the structures are in very nice agreement with the structures determined by global optimization methods performed at 0 K,[28,29] proving that freezing simulations are effective in finding the minimum energy structures. This study gives not only the ground state at 0 K, but also the temperature-dependent variations of the structures. These are important when comparing with experiments that are performed at finite temperature.

We have shown that for Ag, Pt, and Pd clusters, there is no solid-solid transition with increasing temperature, so that cluster structures are quite stable in terms of epitaxial orientation, structure, morphology, and aspect ratio, except at very high temperature near the melting point where structures may fluctuate. We found that Ag nanoclusters adopt the (100) epitaxy in the whole size range covered by this study (from 200 to 800 atoms), in nice agreement with experimental results.[19,20] For Pt and Pd, the (100) epitaxy dominates for small sizes and there is a transition toward the (111) epitaxy at larger sizes. This can be correlated with the network misfit and the difference in adhesion energies between the two epitaxies. Ag has the smallest misfit (3%) and the largest adhesion energy difference between (100) and (111) (24%); therefore, it keeps the (100) epitaxy. Pt and Pd have larger misfit (7% and 8%) and much lower adhesion energy difference (7% and 6%), so that they change epitaxy with increasing cluster size and Pd changes at smaller size than Pt. The comparison with experimental results is less good than with Ag. Indeed, even if the GISAXS study of Pt nanoclusters[22] displays
the two kinds of epitaxies, the transition toward (111) as a function of size has not been clearly evidenced. In the case of Pd, there is practically no evidence of (111) epitaxial structures[15,16] or in marginal cases. This disagreement may be due to two reasons: the approximations assumed in our model and the interplay between growth and equilibrium in the experiments.

(i) We have shown that the driving forces that control the epitaxial transition are very sensitive to energy variations (either in the adhesion energy or in the anisotropy of the metal surface energy). We guess that with a slightly modified energetic model, the transition size could be shifted significantly, without changing significantly the qualitative effects that have been described in that study. This is effectively the case if we use the TB-SMA potential extended to the third neighbors which has been fitted in order to improve the stacking fault energy. In fact it also improves the surface energy and leads to a shift of the (100)-(111) epitaxial transition from 200 atoms to about 800 atoms,[29] which is still too small in size (3.5 nm) but goes in the good direction.

(ii) From the experimental point of view, it is worth noticing that the nanoparticles observed in the experiments are usually in growth conditions, which means that even if the growth is performed at quite high temperature (from 550 to 740 K)[16] the epitaxial orientation as well as the aspect ratio can be trapped by kinetic effects, preventing the comparison with equilibrium structures. As the (100) epitaxy is the one

adopted at small sizes, such epitaxy may persist during the growth. In fact, in the experimental conditions (time and temperature), the energetic barrier from the (100) to the (111) epitaxy may not be overcome (such barrier increases with cluster size).

Another difficulty when comparing experiments to theory is the coalescence process which can alter the equilibrium shape measurements during the growth. There are a few experiments that have measured the aspect ratio of clusters at very low metal deposited thickness, preventing coalescence effects on Ag (Ref. 20) and Pd.[16] The experimental aspect ratios are in very good agreement with our theoretical prediction in the case of Ag/MgO(100) and is underestimated by our model in the case of Pd because the surface energy of Pd is significantly underestimated. We already showed that modifying the potential in order to improve the Pd surface energy leads to a better aspect ratio estimation[18] which is in better agreement with the experimental result. This is also the case of the TB-SMA potential extended to the third neighbors used here. We show that the WK construction gives a quite reasonable idea of the aspect ratio of the nanoparticles (when they are not too small) in order to use it as an efficient method to measure the adhesion energy in the experiments. However we show also that such adhesion energy is susceptible to vary with decreasing size because of epitaxial strain which leads to some variations of the aspect ratio at small sizes, independently of discontinuous character coming from the discretization of the length with atomic layers.

To conclude, this study has shown that the simulation of the recrystallization of metallic nanodroplets supported on MgO(100) surface by canonical MD was able to determine the main aspects of the structure of nanoclusters as compared to 0 K optimized structures.[28,29] This is a step to validate such method as a way to give equilibrium structures even if coming from dynamics simulations. The key point is the large surface/bulk ratio which, thanks to the easy surface diffusion, allows us to fulfill the ergodicity condition. Once we get such equilibrium states, this study goes beyond 0 K optimized structures since it can give the characterization of finite-temperature equilibrium structures to be compared directly with experimental results. In the cases we have studied here, i.e., Pd, Pt, and Ag nanoclusters on MgO(100) surface, the main structural and morphological aspects and notably the epitaxial relation with the support are not influenced by the temperature, so that the 0 K optimized structures[28,29] can be reasonably considered as the good structures to be compared to the experimental ones. However, in the Pt case where we did not obtain a clear epitaxial transition in the size range from 91 up to 807 atoms (also because the energies of the two structures are quasidegenerated), we cannot exclude temperature effects that would modify the structural stability as compared to 0 K structures and could favor the (100) epitaxy to larger sizes than the ones expected at 0 K. This could explain, beyond growth conditions restrictions, why experimental results at 1000 K find systematically the (100) epitaxy.[22]

ACKNOWLEDGMENTS

We acknowledge financial support from the French National Agency for Research under the project SIMINOX (Grant No. ANR-06-NANO-009-01) and from l'Oréal Italia e UNESCO per le Donne e la Scienza, 2007 edition.

*Also at Institute of Physical Chemistry "IG Murgulescu," Romanian Academy, Spl. Independentei 202, Bucharest, Romania.

[1] C. T. Campbell, Surf. Sci. Rep. **27**, 1 (1997).
[2] C. R. Henry, Surf. Sci. Rep. **31**, 231 (1998).
[3] S. Giorgio, C. R. Henry, C. Chapon, and J. M. Penisson, J. Cryst. Growth **100**, 254 (1990).
[4] B. Pauwels, G. Van Tendeloo, W. Bouwen, L. T. Kuhn, P. Lievens, H. Lei, and M. Hou, Phys. Rev. B **62**, 10383 (2000).
[5] H. Graoui, S. Giorgio, and C. R. Henry, Philos. Mag. B **81**, 1649 (2001).
[6] A. Piednoir, E. Perrot, S. Granjeaud, A. Humbert, C. Chapon, and C. R. Henry, Surf. Sci. **391**, 19 (1997).
[7] K. Hojrup Hansen, T. Worren, S. Stempel, E. Laegsgaard, M. Baumer, H.-J. Freund, F. Besenbacher, and I. Stensgaard, Phys. Rev. Lett. **83**, 4120 (1999).
[8] T. Worren, K. Hojrup Hansen, E. Laegsgaard, F. Besenbacher, and I. Stensgaard, Surf. Sci. **477**, 8 (2001).
[9] S. Ferrero, A. Piednoir, and C. R. Henry, Nano Lett. **1**, 227 (2001).
[10] O. H. Pakarinen, C. Barth, A. S. Foster, and C. R. Henry, J. Appl. Phys. **103**, 054313 (2008).
[11] G. Renaud, Surf. Sci. Rep. **32**, 5 (1998).
[12] H. Graoui, S. Giorgio, and C. R. Henry, Surf. Sci. **417**, 350 (1998).
[13] G. Renaud, A. Barbier, and O. Robach, Phys. Rev. B **60**, 5872 (1999).
[14] F. Leroy, C. Revenant, G. Renaud, and R. Lazzari, Appl. Surf. Sci. **238**, 233 (2004).
[15] G. Renaud, R. Lazzari, C. Revenant, A. Barbier, M. Noblet, O. Ulrich, F. Leroy, J. Jupille, Y. Borensztein, C. R. Henry, J.-P. Deville, F. Scheurer, J. Mane-Mane, and O. Fruchart, Science **300**, 1416 (2003).
[16] C. Revenant, F. Leroy, R. Lazzari, G. Renaud, and C. R. Henry, Phys. Rev. B **69**, 035411 (2004).
[17] C. R. Henry, Prog. Surf. Sci. **80**, 92 (2005).
[18] C. Mottet and J. Goniakowski, J. Comput. Theor. Nanosci. **4**, 326 (2007).
[19] O. Robach, G. Renaud, and A. Barbier, Phys. Rev. B **60**, 5858 (1999).
[20] C. Revenant, G. Renaud, R. Lazzari, and J. Jupille, Nucl. Instrum. Methods Phys. Res. B **246**, 112 (2006).
[21] C. Gatel, P. Baules, and E. Snoeck, J. Cryst. Growth **252**, 424 (2003).
[22] J. Olander, R. Lazzari, J. Jupille, B. Mangili, J. Goniakowski, and G. Renaud, Phys. Rev. B **76**, 075409 (2007).
[23] M. Marsault, G. Hamm, A. Worz, G. Sitja, C. Barth, and C. R. Henry, Faraday Discuss. **138**, 407 (2008).
[24] J. Oviedo, J. F. Sanz, N. Lopez, and F. Illas, J. Phys. Chem. B

104, 4342 (2000).
[25] N. C. Hernandez and J. F. Sanz, J. Phys. Chem. B **105**, 12111 (2001).
[26] M. A. San-Miguel, J. Oviedo, and J. F. Sanz, Phys. Rev. Lett. **99**, 066102 (2007).
[27] F. Baletto and R. Ferrando, Rev. Mod. Phys. **77**, 371 (2005).
[28] R. Ferrando, G. Rossi, A. C. Levi, Z. Kuntova, F. Nita, A. Jelea, C. Mottet, G. Barcaro, A. Fortunelli, and J. Goniakowski, J. Chem. Phys. (to be published).
[29] J. Goniakowski, A. Jelea, C. Mottet, G. Barcaro, A. Fortunelli, Z. Kuntova, F. Nita, A. C. Levi, G. Rossi, and R. Ferrando J. Chem. Phys. (to be published).
[30] V. Rosato, M. Guillopé, and B. Legrand, Philos. Mag. A **59**, 321 (1989).
[31] J. Friedel, in *The Physics of Metals*, edited by J. M. Ziman (Cambridge University Press, Cambridge, England, 1969), p. 340.
[32] C. Kittel, *Introduction to Solid State Physics*, 7th ed. (Wiley, New York, 1996).
[33] G. Simmons and H. Wang, *Single Crystal Elastic Constants and Calculated Aggregated Properties* (MIT, Cambridge, MA, 1971).
[34] M. S. Daw and M. I. Baskes, Phys. Rev. Lett. **50**, 1285 (1983).
[35] K. W. Jacobsen, J. K. Norskov, and M. J. Puska, Phys. Rev. B **35**, 7423 (1987).
[36] J. P. Perdew and Y. Wang, Phys. Rev. B **45**, 13244 (1992).
[37] I. L. Dillamore and R. E. Smallman, Philos. Mag. **12** 191 (1965); C. B. Carter and S. M. Holmes, *ibid.* **35**, 1161 (1977); H. Saka, T. Iwata, and T. Imura, Philos. Mag. A **37**, 273 (1978).
[38] R. Ferrando, G. Rossi, F. Nita, G. Barcaro, and A. Fortunelli, ACS Nano **2**, 1849 (2008).
[39] http://cms.mpi.univie.ac.at/vasp/
[40] C. Noguera, *Physics and Chemistry at Oxide Surfaces* (Cambridge University Press, Cambridge, England, 1995).
[41] M. W. Finnis, J. Phys.: Condens. Matter **8**, 5811 (1996).
[42] J. Goniakowski, C. Mottet, and C. Noguera, Phys. Status Solidi B **243**, 2516 (2006).
[43] L. Spiess, Surf. Rev. Lett. **3**, 1365 (1996).
[44] E. Heifets, Yu. F. Zhukovskii, E. A. Kotomin, and M. Causa, Chem. Phys. Lett. **283**, 395 (1998); Yu. F. Zhukovskii, E. A. Kotomin, P. W. M. Jacobs, and A. M. Stoneham, Phys. Rev. Lett. **84**, 1256 (2000); Yu. F. Zhukovskii, E. A. Kotomin, D. Fuks, S. Dorfman, and A. Gordon, Surf. Sci. **482**, 66 (2001).
[45] J. A. Purton, D. M. Bird, S. C. Parker, and D. W. Bullett, J. Chem. Phys. **110**, 8090 (1999).
[46] J. Goniakowski, Phys. Rev. B **57**, 1935 (1998); **58**, 1189 (1998); **59**, 11047 (1999).
[47] N. Lopez and F. Illas, J. Phys. Chem. B **102**, 1430 (1998).
[48] L. Giordano and G. Pacchioni, Surf. Sci. **575**, 197 (2005).
[49] L. Xu, G. Henkelman, C. T. Campbell, and H. Jonsson, Surf. Sci. **600**, 1351 (2006).
[50] G. Barcaro and A. Fortunelli (private communication).
[51] http://www.pwscf.org/
[52] W. Vervisch, C. Mottet, and J. Goniakowski, Phys. Rev. B **65**, 245411 (2002).
[53] G. Barcaro and A. Fortunelli, J. Chem. Theory Comput. **1**, 972 (2005).
[54] http://www.cinam.univ-mrs.fr/mottet/param/metalMgO.pdf
[55] W. Vervisch, C. Mottet, and J. Goniakowski, Eur. Phys. J. D **24**, 311 (2003).
[56] H. C. Andersen, J. Chem. Phys. **72**, 2384 (1980).
[57] D. Frenkel and B. Smit, *Understanding Molecular Simulations: From Algorithms to Applications* (Academic, New York, 1996).
[58] H. F. Busnengo, W. Dong, P. Sautet, and A. Salin, Phys. Rev. Lett. **87**, 127601 (2001).
[59] J. Goniakowski and C. Mottet, J. Cryst. Growth **275**, 29 (2005).
[60] C. Mottet and J. Goniakowski, Surf. Sci. **566-568**, 443 (2004).
[61] J. D. Honeycutt and H. C. Andersen, J. Phys. Chem. **91**, 4950 (1987).
[62] D. Faken and H. Jonsson, Comput. Mater. Sci. **2**, 279 (1994).
[63] Y. F. Zhukovskii, M. Alfredsson, K. Hermansson, E. Heifets, and E. A. Kotomin, Nucl. Instrum. Methods Phys. Res. B **141**, 73 (1998).